The Influence of Soil Moisture on the Historic 2021 Pacific Northwest Heatwave

ROBERT CONRICK^a AND CLIFFORD F. MASS^a

^a Department of Atmospheric Sciences, University of Washington, Seattle, Washington

(Manuscript received 16 September 2022, in final form 2 February 2023)

ABSTRACT: During late June 2021, a record-breaking heatwave impacted western North America, with all-time high temperatures reported across Washington, Oregon, British Columbia, and Alberta. The heatwave was forced by a highly anomalous upper-level ridge, strong synoptic-scale subsidence, and downslope flow resulting in lower-tropospheric adiabatic warming. This study examines the impact of antecedent soil moisture on this extreme heat event. During the cool season of 2020/21, precipitation over the Pacific Northwest was above or near normal, followed by a dry spring that desiccated soils to 50%–75% of normal moisture content by early June. Low surface soil moisture affects the surface energy balance by altering the partitioning between sensible and latent heat fluxes, resulting in warmer temperatures. Using numerical model simulations of the heatwave, this study demonstrates that surface air temperatures were warmed by an average of 0.48°C as a result of dry soil moisture conditions, compared to a high-temperature anomaly of 10°–20°C during the event. Air temperatures over eastern Washington and southern British Columbia were most sensitive to soil moisture anomalies, with 0000 UTC temperature anomalies ranging from 1.2° to 2.2°C. Trajectory analysis indicated that rapid subsidence of elevated parcels prevented air parcels from being affected by surface heat fluxes over a prolonged period of time, resulting in a relatively small temperature sensitivity to soil moisture. Changes to soil moisture also altered regional pressure, low-level wind, and geopotential heights, as well as modified the marine air intrusion along the Pacific coast of Washington and Oregon.

SIGNIFICANCE STATEMENT: The record-breaking western North American heatwave of late June 2021 was preceded by below-normal soil moisture over the region. This study evaluates the role of soil moisture on the 2021 heatwave, demonstrating that the anomalous temperatures during this extreme event were not significantly increased by below-normal soil moisture.

KEYWORDS: Atmosphere-land interaction; Extreme events; Heat wave; Mesoscale models; Model evaluation/performance

1. Introduction

The land surface exerts a significant influence over nearsurface sensible weather. For example, soil moisture is an important driver of near-surface air temperature and humidity through its modulation of sensible and latent heat fluxes (e.g., Seneviratne et al. 2010; Schwingshackl et al. 2017; Liu and Pu 2019). The correlation between soil dryness and low-level air temperature is positive (e.g., Huang and van den Dool 1993; Jia et al. 2019; Fischer et al. 2007; Hirschi et al. 2011; Miralles et al. 2012; Hirsch et al. 2014). Surface-based evaporation cools the atmosphere above by enhancing the latent heat flux and reducing the sensible heat flux. In contrast, dry soils warm more rapidly resulting in greater sensible heat flux. This relationship between soil moisture and air temperature has been demonstrated for a variety of geographic locales, land surface types, and meteorological conditions (e.g., Lakshmi et al. 2003; Koster et al. 2004; Seneviratne et al. 2006; Koster et al. 2009; Jaeger and Seneviratne 2011; Taylor et al. 2012; Seneviratne et al. 2013; Whan et al. 2015; Petch et al. 2020).

As a result of the relationship between soil moisture and surface heat fluxes, the extreme warmth associated with heatwaves is modulated by soil moisture (Miralles et al. 2012,

Corresponding author: Robert Conrick, robert.conrick@gmail.com

2014, 2019). For example, Fischer et al. (2007) found that Europe's record-breaking 2003 summer heatwave was as much as 4°C warmer due to a prolonged antecedent precipitation deficit over most of continental Europe. Another study by Petch et al. (2020) showed that dry soil contributed approximately 1°C to the historic 2018 Great Britain heatwave. Other studies have shown that heatwaves are often linked to dry soil moisture conditions, such as in Europe (Brabson et al. 2005; Hirschi et al. 2011; Stéfanon et al. 2014; Dirmeyer et al. 2021; Petch et al. 2020), China (Meng and Shen 2014), Australia (Cai et al. 2009; Hirsch et al. 2014), and the contiguous United States (Durre et al. 2000; Alfaro et al. 2006; Ford and Quiring 2014; Benson and Dirmeyer 2021). With the frequency and severity of heatwaves projected to increase (e.g., Perkins et al. 2012; Mazdiyasni and AghaKouchak 2015; Sheridan and Lee 2018; Yu et al. 2020), accompanied by changing global precipitation patterns (e.g., Putnam and Broecker 2017), it is important to investigate the role of soil moisture on high-impact heatwave events.

During late June 2021, a record-breaking heatwave affected western North America, including the states of Washington and Oregon in the United States as well as the Canadian provinces of British Columbia and Alberta. During the event there were several days of maximum temperatures 10°–20°C above normal, with the heat associated with a highly anomalous upper-level ridge and strong subsidence in the lower

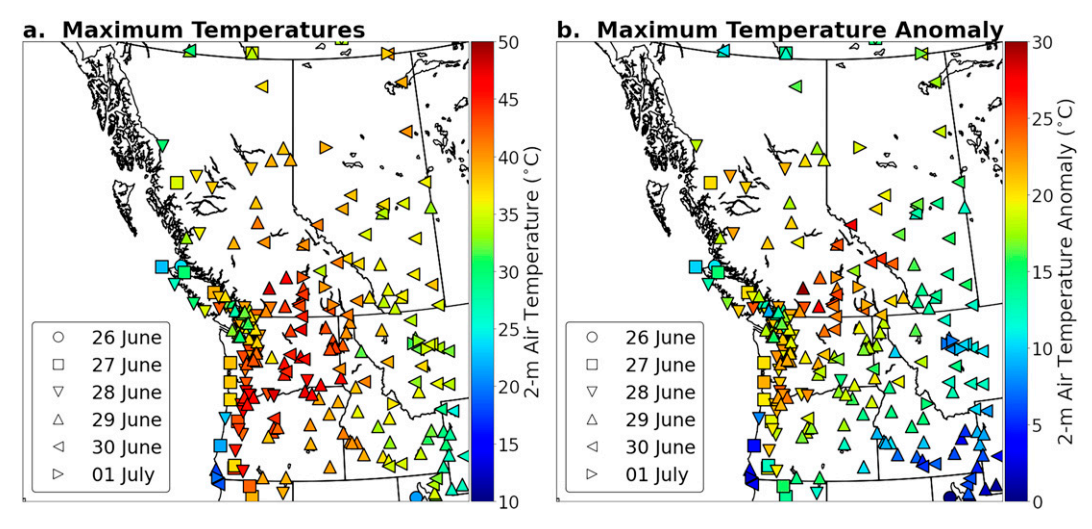


FIG. 1. (a) Maximum 2-m air temperatures and (b) maximum temperature anomalies observed during the heatwave (26 Jun–1 Jul 2021). Colors indicate the magnitude of maximum air temperature, and the icon shape indicates on which day that maximum air temperature occurred.

troposphere (Overland 2021). Before the heatwave, a March-June precipitation deficit reduced soil moisture over the region, leading several studies to speculate about the influence of soil moisture during the 2021 Pacific Northwest heatwave (Neal et al. 2022; Overland 2021; Thompson et al. 2022), though none of these studies directly quantified the role of soil moisture. One recent study by Bartusek et al. (2022) concluded that the 2021 heatwave was amplified by as much as 40% due to land-atmosphere feedbacks. During the June 2021 heatwave, large portions of Washington, Oregon, and British Columbia experienced air temperatures exceeding 40°C and high temperature anomalies exceeding 20°C (Fig. 1). Many of the region's major urban areas recorded all-time record or near-record high temperatures, including Calgary (AB; 36.3°C, 97.3°F), Edmonton (AB; 37.4°C, 99.3°F), Portland (OR; 46.7°C, 116°F), Seattle (WA; 42.2°C, 108°F), and Spokane (WA; 42.8°C, 109°F). Canada's all-time highest temperature (49.6°C, 121.3°F) was recorded in Lytton (BC), approximately 150 km northeast of Vancouver.

The goals of this study include: 1) to document the evolution of precipitation and soil moisture deficits before the start of the 2021 Pacific Northwest heatwave, and 2) to examine the role of dry soils in contributing to the extreme heatwave. To accomplish these goals, we first describe the synoptic and surface conditions associated with the heatwave, including precipitation and soil moisture conditions during the months preceding the event. Numerical simulations initialized with climatological and observed soil moisture conditions are then used to quantify the temperature and circulation impacts of the antecedent soil moisture deficit.

2. Overview of the historic June 2021 heatwave

a. Synoptic overview

The June 2021 heatwave was strongly forced by highly anomalous 500-hPa ridging over the northeast Pacific Ocean

that developed starting 24 June and subsequently extended over the U.S. Pacific Northwest, British Columbia, and Alberta over the next 48 h (Fig. 2). Standardized 500-hPa height anomalies¹ exceeded $+4\sigma$ during the event, with anomalies peaking around 0000 UTC 27 June (Fig. 2c). This anomalous upper-level ridge slowly translated eastward from 26 June to 2 July, by which time the heatwave had generally ended across the U.S. Pacific Northwest, British Columbia, and Alberta. Along with lower-tropospheric subsidence associated with anomalous midtropospheric ridging, the location of the ridge and its near-surface reflection promoted downslope winds and associated subsidence warming on the lee (generally western) side of regional terrain (e.g., the Cascade Mountains and the Canadian Rockies), as indicated by the wind anomalies in Fig. 2.

HYSPLIT² (Stein et al. 2015) 72-h backward air parcel trajectories ending at 500 m AGL above Seattle, Spokane, and a location ~200 km west of Edmonton are shown in Fig. 3 at 0000 UTC 29 June, 0000 UTC 30 June, and 0000 UTC 1 July, corresponding to the warmest periods at each location.

Air parcels ending above Seattle and Spokane on 29 June followed an anticyclonic path around the ridge as they subsided from their starting location more than 3 km AGL above northern British Columbia. Parcels remained aloft (but slowly subsiding) until crossing the western slopes of the Rocky Mountains, after which they descended rapidly toward the

¹ Based on the 1980–2020 climatology. "Standardized anomalies" are anomalies normalized by the regional climatology, which converts the distribution to a normal distribution. It is defined as $N=(X-\mu)/\sigma$, where X is the value, μ is the mean, and σ is the standard deviation at each grid point. The resulting normalization is interpreted as the number of standard deviations from the climatological mean.

² The HYSPLIT trajectories shown are forced with the National Center for Environmental Prediction (NCEP) Global Data Assimilation System (GDAS) analysis.

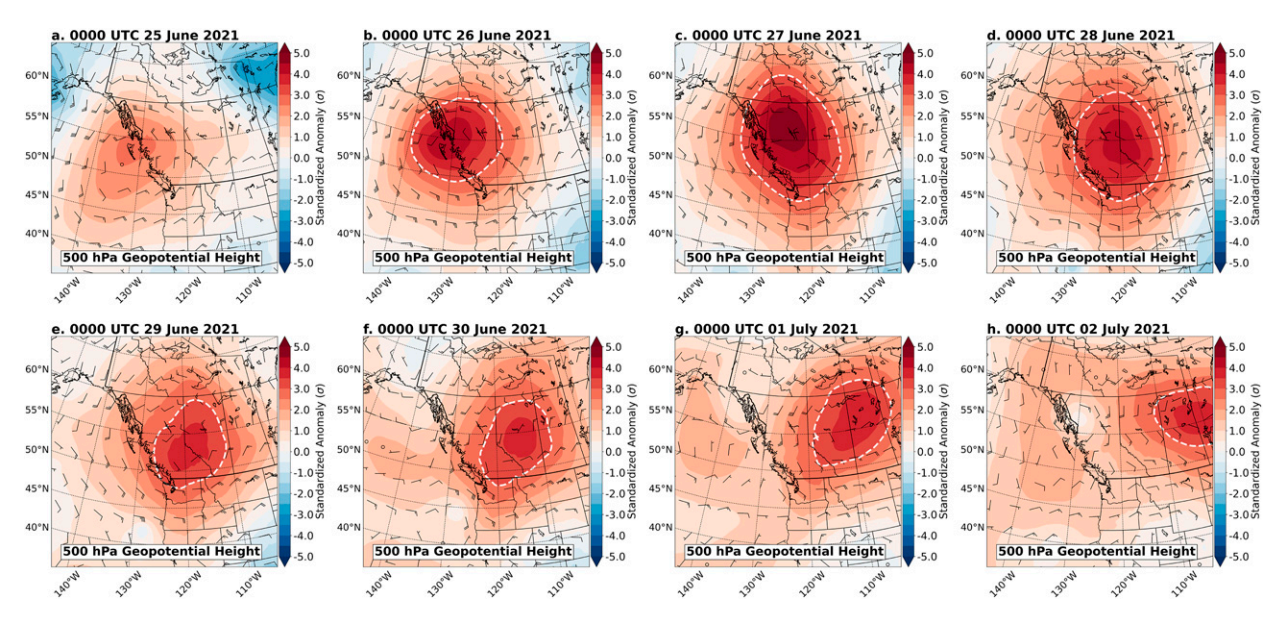


FIG. 2. Standardized anomalies of 500-hPa geopotential height over western North America during the evolution of the heatwave. The dashed white line indicates the +3 standard deviation contour. Wind barbs show wind anomalies at 500 hPa (m s⁻¹; half barb = 5 m s⁻¹). Data are from ERA5 (Hersbach et al. 2020).

surface over central and eastern Washington. Air parcels ending over Seattle at the later times remained close to the surface and originated offshore, reflecting the influx of marine air that ended the heatwave on 29 June for areas along the Pacific Coast.

The air parcel trajectory ending near Edmonton, east of the Canadian Rockies, where the warmest temperatures occurred on 30 June–1 July, remained close to the surface on 29 June and exhibited erratic motion consistent with a location near the center of the event's anomalous ridge. In contrast, at the later times, the air parcel trajectories ending near Edmonton were qualitatively similar to those ending at Spokane, beginning at more than 3 km AGL before subsiding to the surface.

Those parcels ending at 0000 UTC 30 June remained above 1.5 km AGL until passing over the eastern slopes of the Canadian Rockies and then rapidly descended, whereas the parcels ending at 0000 UTC 1 July were less influenced by terrain and more gradually subsided toward the surface.

The combination of subsidence in the free troposphere, subsidence on the lee side of regional topography, and strong solar heating near the summer solstice contributed to the extreme positive temperature anomalies over the region (Overland 2021; Thompson et al. 2022; Wang et al. 2023). Low-level (2-m) air temperature anomalies from the 1980 to 2020 climatology exceeded $+4\sigma$ over large portions of Washington, British Columbia, and western Alberta (Fig. 4). Three regions

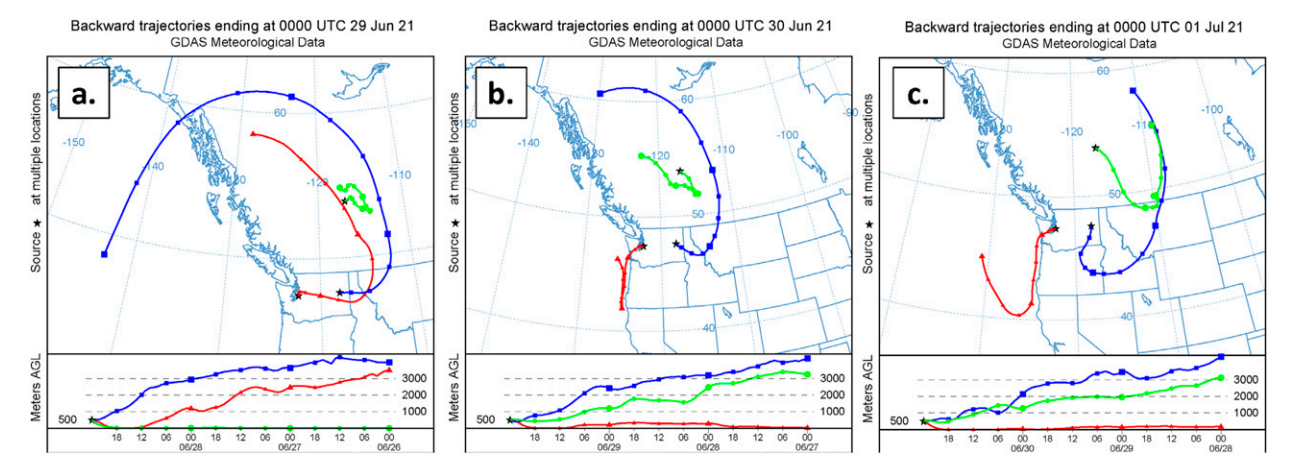


FIG. 3. (top) Air parcel 72-h back trajectories from the NOAA HYSPLIT model ending (a) 0000 UTC 29 Jun, (b) 0000 UTC 30 Jun, and (c) 0000 UTC 1 Jul 2021. The red trajectory ends at Seattle (WA), the blue trajectory ends at Spokane (WA), and the green trajectory ends ~200 km west of Edmonton (AB). (bottom) Each trajectory's altitude above ground level (m AGL). The HYSPLIT model was forced with GDAS meteorological data.

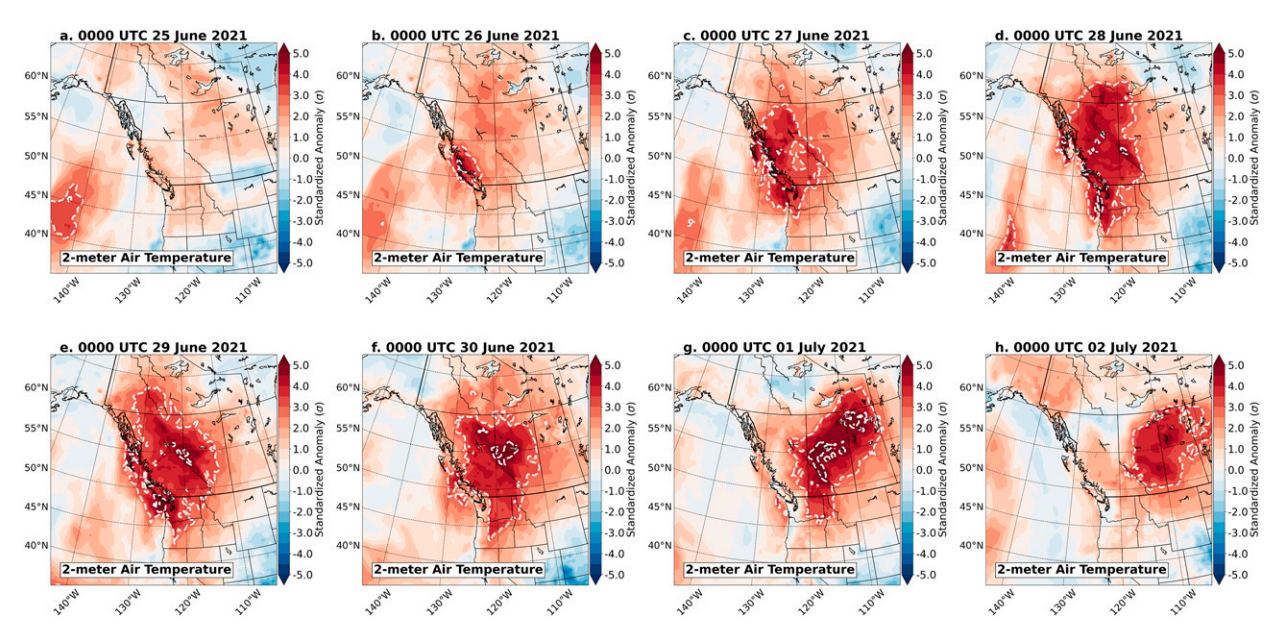


FIG. 4. Standardized anomalies of 2-m air temperature over western North America throughout the evolution of the heatwave. The dashed white lines encircle the +3 and +5 standard deviation (σ) contours. Data are from ERA5 (Hersbach et al. 2020).

downstream of topography (the western slopes of the Cascades, the Coast Mountains of British Columbia, and the Canadian Rockies) were particularly susceptible to downslope adiabatic warming as a result of clockwise flow around the upper-level ridge impinging perpendicularly on the north–south orientation of those mountain ranges.

As the upper-level ridge and its surface reflection advected eastward, the heatwave first weakened west of the Cascade crest over coastal Washington and Oregon and then declined a few days later over eastern Washington, British Columbia, and Alberta. Along the Washington and Oregon coastal zone, temperatures began to decline on 29 June as marine air (a marine push) surged inland (Mass et al. 1986; Jannuzzi 1993). Section 4 discusses how soil moisture affected the event's marine push.

b. Precipitation and soil moisture

Precipitation and soil moisture exhibited a drying trend during the 180 days prior to the start³ of the heatwave (Fig. 5). Starting with precipitation, conditions were near or above normal during the 120–180 days (December 2020–February 2021) before the heatwave for the southern and western portions of the domain, while western Washington and western British Columbia experienced slightly below-normal precipitation (70%–90% of climatology; Fig. 5a). Conditions became much drier across the region during the 30–120 days prior to the heatwave (February 2021–May 2021; Fig. 5c). All of the U.S. Pacific Northwest and the southern half of British Columbia received less (50%–80%) precipitation than normal during this period, with the greatest deficit over portions of eastern Washington, which received less than 50% of normal precipitation. Finally,

the period 1–30 days prior to the heatwave (May 2021–June 2021; Fig. 5e) was exceptionally dry over nearly all of the region, with the exception of far northwestern British Columbia and northern Alberta. For coastal areas of Washington and Oregon, precipitation was at or slightly above normal at the start of the heatwave due to a convective precipitation event 10–14 days prior to the start of the event. Soil moisture approximately mirrored the behavior of precipitation during the 180-day period before the heatwave began (Figs. 5b,d,e). For 1–30 days prior to the start of the heatwave, soil moisture deficits were largest over eastern Washington, southern British Columbia, and southern Alberta (Fig. 5d).

The following sections apply a pair of numerical experiments to examine the meteorological impacts of the observed below-normal soil moisture immediately prior to the heatwave. Specifically, we compare two simulations: one uses the observed (drier-than-normal) soil moisture and the second applies climatological (moister-than-observed) conditions.

3. Model configuration and data sources

a. Model configuration

To explore the role of soil moisture on the June 2021 heatwave, we employed the Weather Research and Forecasting Model (WRF-ARW; Skamarock et al. 2008) version 4.1.3. The model was run from 1200 UTC 26 June to 1200 UTC 2 July 2021, a period encompassing the development, peak, and decay of the heatwave.

A 36–12–4-km nested domain configuration was used. The innermost domain (4-km horizontal grid spacing) covered all of the U.S. Pacific Northwest, British Columbia, Alberta, and a portion of the northeastern Pacific Ocean (Fig. 6). The WRF hybrid vertical coordinate option (Klemp 2011) was

³ The start of the heatwave is chosen as 1200 UTC 26 June 2021 based on Fig. 3.

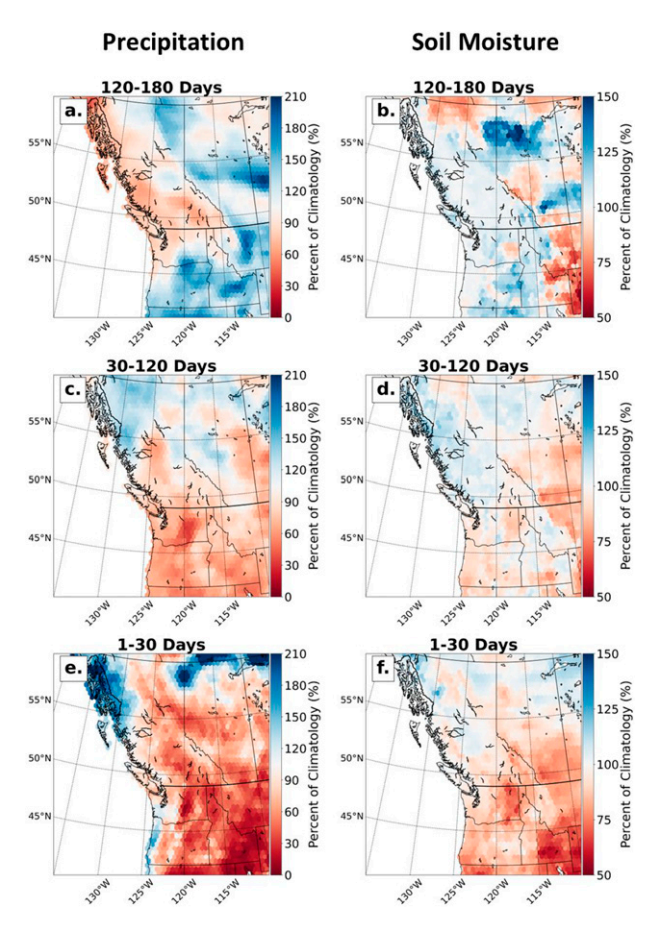


FIG. 5. Percent of climatology (1980–2020) for (left) precipitation based on ERA5 (Hersbach et al. 2020) and (right) 0–10-cm soil moisture from the Global Land Data Assimilation System (GLDAS; Rodell et al. 2004) averaged for (a),(b) 120–180; (e),(f) 30–120; and (c),(d) 1–30 days before the heatwave.

applied to 38 unequally spaced vertical levels, with the sigmaisobaric transition level set at its default value of 0.2.

Model initial and boundary conditions were from Global Forecast System (GFS) analyses. The outer boundaries were updated every 6 h and the outer domain was nudged toward the analysis using the WRF four-dimensional data assimilation (FDDA) grid nudging scheme. Other model configuration options included the RRTMG longwave and shortwave radiation parameterization (Iacono et al. 2008), the Yonsei University (YSU) planetary boundary and surface layer scheme (Hong et al. 2006), the Grell–Freitas cumulus parameterization (Grell and Freitas 2014), and the Thompson et al. (2008) microphysical parameterization. To represent the state of the land surface during the simulations, the Noah land surface model (Ek et al. 2003) was used.

b. Meteorological data

To evaluate our WRF simulations, near-surface (2-m) air temperature data were obtained from NOAA/FAA Automated Surface Observing Stations (ASOS/AWOS) sites and surface stations maintained by Environment Canada within

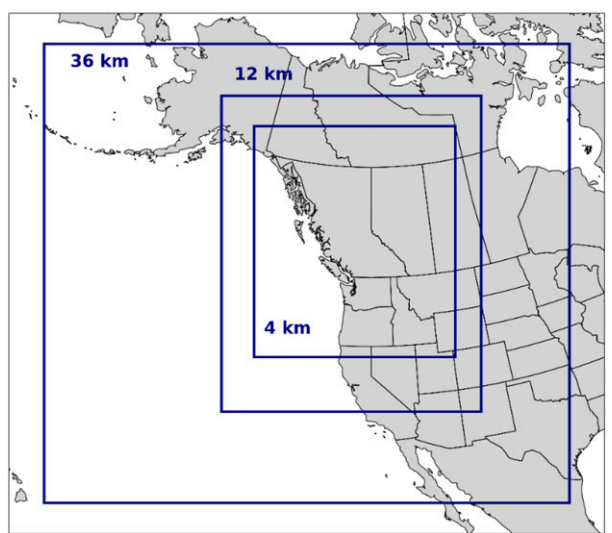


FIG. 6. WRF-ARW Model domains used in this study.

the 4-km domain. Additional information about these stations, including siting and accuracy specifications, is provided in the ASOS User Guide⁴ or the Environment and Climate Change Canada MANOBS document.⁵ Only the highest-quality stations located at airports were included. Air temperature data were subjected to the quality control procedures of the National Centers for Environmental Prediction (NCEP) Meteorological Assimilation Data Ingest System (MADIS).⁶ Rawinsonde observations from Quillayute (WA), Spokane (WA), Salem (OR), Medford (OR), Boise (ID), Port Hardy (BC), Prince George (BC), Vernon (BC), and Edmonton (AB) were also obtained to evaluate model performance. Locations of all observing sites used by this study are shown in Fig. 7. Rawinsonde and air temperature observations were used to evaluate our simulation, with results shown in appendix A.

c. Soil moisture data and experiments

The model's initial soil moisture conditions were obtained from the Global Land Data Assimilation System (GLDAS; Rodell et al. 2004). GLDAS uses a combination of observations (surface and satellite) and gridded analyses to drive several land surface models at high spatial and temporal resolution over an extended period (1948–present). For consistency with our model configuration, we used the 0.25° 3-h Noah LSM implementation of GLDAS, applying the default soil levels of the Noah LSM: 0–10-, 10–40-, 40–100-, and 100–200-cm layers. This is the same GLDAS dataset used in our description of soil moisture conditions from section 2. Hereafter, all soil moisture analysis will refer to the uppermost layer (0–10-cm depth), due to its significant impact on short-term near-surface weather (Xu et al. 2021). More information about the GLDAS system can

⁴ https://www.weather.gov/media/asos/aum-toc.pdf.

⁵ https://publications.gc.ca/site/eng/9.907779/publication.html.

⁶ MADIS quality control steps are described in NWS Techniques Specification Package (TSP) 88–21-R2 (1994).

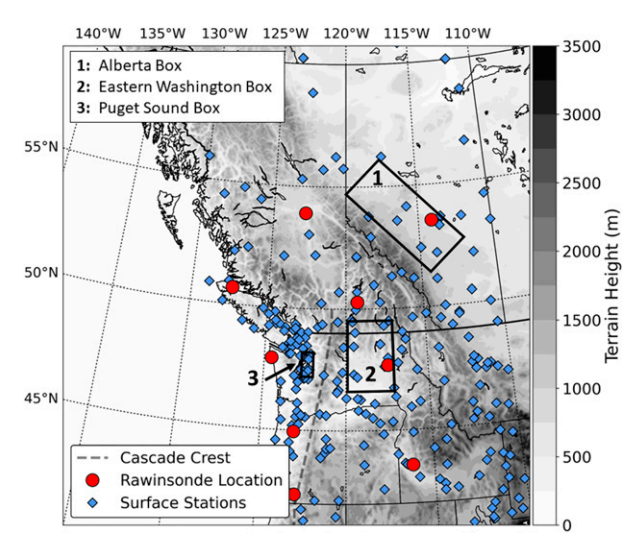


FIG. 7. Surface and rawinsonde station locations used to evaluate the Control simulation. Shading indicates terrain height. The black boxes (numbered; see upper-left legend) are analysis regions and the ending locations of trajectories—these regions are used to examine air temperature differences in section 4.

be found in Rodell et al. (2004) and the NASA Land Data Assimilation System project website.⁷

Two model experiments were formulated to assess the role of soil moisture during the heatwave: the Control and Climo simulations. In the Control simulation, the observed GLDAS soil moisture at 1200 UTC 26 June 2021 is used for the WRF initial soil moisture conditions. In the Climo simulation, a 1200 UTC GLDAS soil moisture climatology (1980-2020) for 26 June 2021 is used to initialize the WRF Model. This experimental design is similar to the study of Fischer et al. (2007), which investigated the 2003 European heatwave. Figure 8 shows the difference between the Control and Climo simulations' initial soil moisture states (1200 UTC 26 June 2021). Consistent with Fig. 5, climatological soil moisture conditions at model initialization are moister in the Climo simulation than the Control over most of the 4-km domain, especially over eastern Washington, southern British Columbia, and western Alberta. Appendix A evaluates the realism of the Control simulation, with results indicating that the simulations were skillful at reproducing observed conditions.

4. Results and discussion

a. Effects on 2-m air temperature

To investigate the contribution of soil moisture content to the heatwave, we compare simulated 2-m air temperatures from the Control and Climo simulations. Averaged over land areas within the 4-km domain from 0000 UTC 26 June to 0000 UTC 1 July 2021, air temperatures were 0.48°C warmer in the Control simulation than the moister Climo simulation (Fig. 9a). Around the warmest time of day, 0000 UTC, air

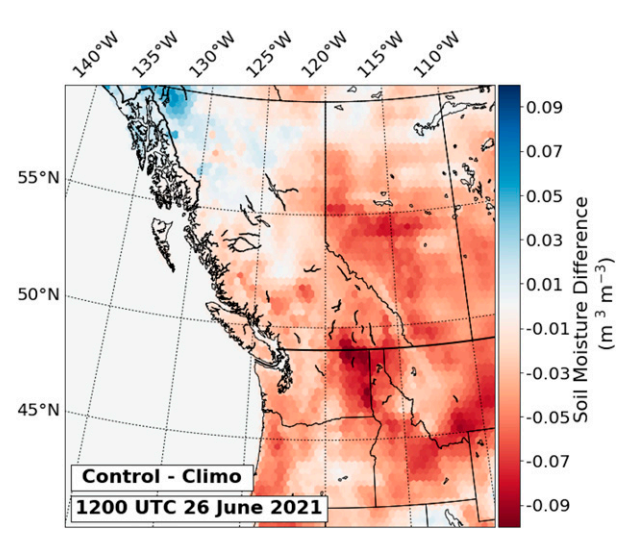


FIG. 8. The 0–10-cm soil moisture difference between climatological and control simulations (Control minus Climo) at the time of model initialization, 1200 UTC 26 Jun 2021.

temperatures were 0.62°C warmer in the Control (Fig. 9b). Mean 0000 UTC temperatures varied considerably throughout the domain, particularly north of 54°N, where differences in diurnal convective activity were evident. Nevertheless, the spatial distribution of average temperature differences closely followed the map of simulated initial soil moisture differences (cf. Figs. 8 and 9). Cooler Control temperatures along the Pacific coast of Washington and Oregon were associated with changes to the alongshore marine air influx, discussed at the end of this section.

Over eastern Washington and west-central Alberta, where soil moisture differences were largest at model initialization, 0000 UTC air temperatures in the Control averaged 1.84° and 1.03°C warmer than the Climo simulation, respectively. Figure 10 shows the 0000 UTC temperature difference between the simulations (Control minus Climo) for the 27 June-1 July period averaged over the analysis boxes in Fig. 7 (eastern Washington, west-central Alberta, and Puget Sound). Over eastern Washington, mean 0000 UTC temperatures in the drier Control simulation were 1.2°-2.3°C warmer than the Climo simulation on all days, peaking on 29 June. The Alberta analysis region warmed by 0.6°-1.5°C with the use of drier soil moisture conditions. Finally, over the Puget Sound region, where the difference between Control and Climo soil moisture was relatively small and air temperatures are affected by marine influences, less warming occurred in the Control compared to the Climo simulation, with 0.2°-1.4°C of warming. In general, dry soil conditions increased 0000 UTC air temperatures by 1%–6% during the heatwave.

The subdued temperature response to soil dryness across the Pacific Northwest can be understood by examining the behavior of surface heat fluxes and air parcel trajectories. Areas where 2-m air temperatures were warmer in the Control relative to Climo were coincident with the greatest increase in sensible heat flux and decrease in latent heat flux (Fig. 11). These locations also had the greatest difference between observed and climatological soil moisture. Specifically, in the dry

⁷ https://ldas.gsfc.nasa.gov/gldas/specifications.

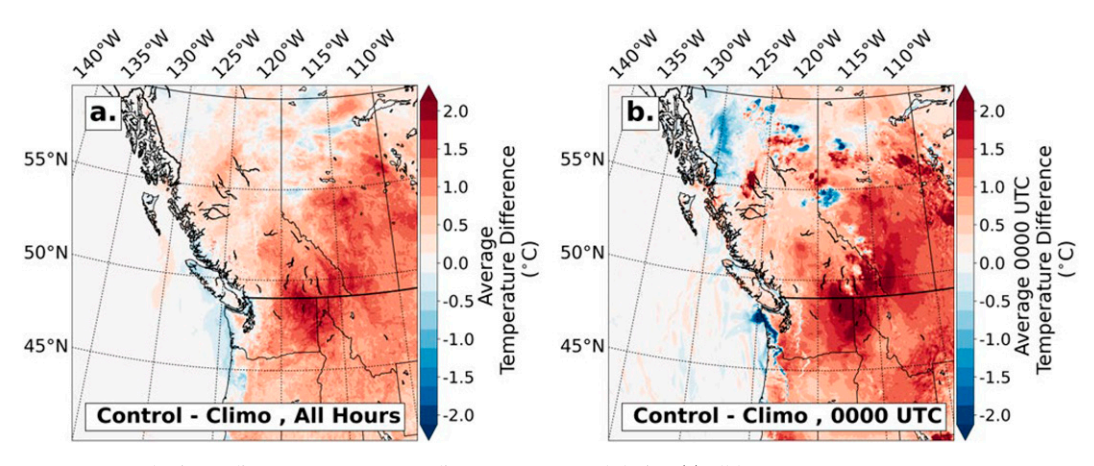


FIG. 9. Control minus Climo 2-m temperature differences averaged during (a) all hours for 0000 UTC 27 Jun-0000 UTC 1 Jul and (b) only 0000 UTC times within the same period.

Control simulation there was a 20–60 W m⁻² decrease in latent heat flux and a coincident sensible heat flux increase of a similar magnitude. Ground heat flux differences (Control minus Climo) averaged less than 2.5 W m⁻². Finally, no significant differences were noted in the mean net surface radiation (±5 W m⁻²) between the Control and Climo simulations. The correspondence between soil moisture, latent–sensible heat partitioning, and cooler near-surface temperatures agrees with both theory and previous studies (e.g., Seneviratne et al. 2010; Schwingshackl et al. 2017; Liu and Pu 2019).

Because of strong subsidence during the heatwave, air parcels reaching the surface originated from the midtroposphere and did not spend a prolonged period close to the surface. As a result, surface fluxes did not exert a large influence on the heatwave. Figure 12 shows the altitudes and paths of Control 30-h backward air parcel trajectories ending at 500 m AGL during the peak of the heatwave, with the three regions outlined in Fig. 7 considered. The heatwave's maximum temperatures occurred around 0000 UTC 29 June for the Puget Sound trajectories (Fig. 12a), while over eastern Washington, southern British Columbia, and western Alberta the maximum temperatures occurred at approximately 0000 UTC 30 June. The majority of trajectories across the three regions and times began above 2500 m AGL and followed a clockwise path while rapidly subsiding until reaching their ending location.

Trajectories from the Control and Climo simulations both followed similar paths, as outlined in appendix B.

To better understand the role of boundary layer processes during the heatwave, we consider the average behavior of trajectories ending over eastern Washington and southern British Columbia (Fig. 13). At 6–30 h before arriving at their ending locations, parcels were near the top of the boundary layer, where fluxes would have minimal impact, or above the boundary layer, where surface heat fluxes would have no impact. Only during the last 6 h of the trajectories were air parcels within the boundary layer and close enough to the surface to be appreciably impacted by boundary layer processes. Appendix B shows that trajectories ending at the other locations shown in Fig. 12 followed a similar evolution. It appears that the limited amount of time that air parcels were in close proximity to the surface was an important factor in minimizing the impact of dry soils on air temperatures.

b. Simulated synoptic/mesoscale differences

It is interesting to hypothesize that changes in heat fluxes and temperatures had an impact on air pressure and wind that might provide an indirect feedback associated with the different soil moisture conditions. In the drier Control simulation, surface air pressure and geopotential heights were reduced by the warmer low-level air temperatures, with the greatest effects within the

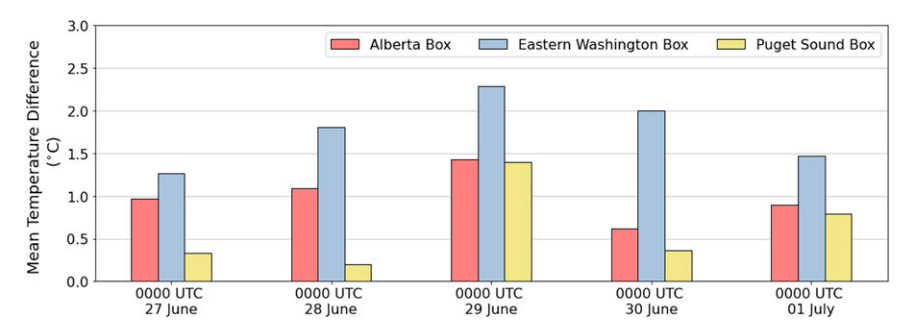


FIG. 10. The 0000 UTC simulated 2-m temperature difference (Control minus Climo) within the analysis boxes shown in Fig. 7 (eastern Washington, west-central Alberta, and Puget Sound).

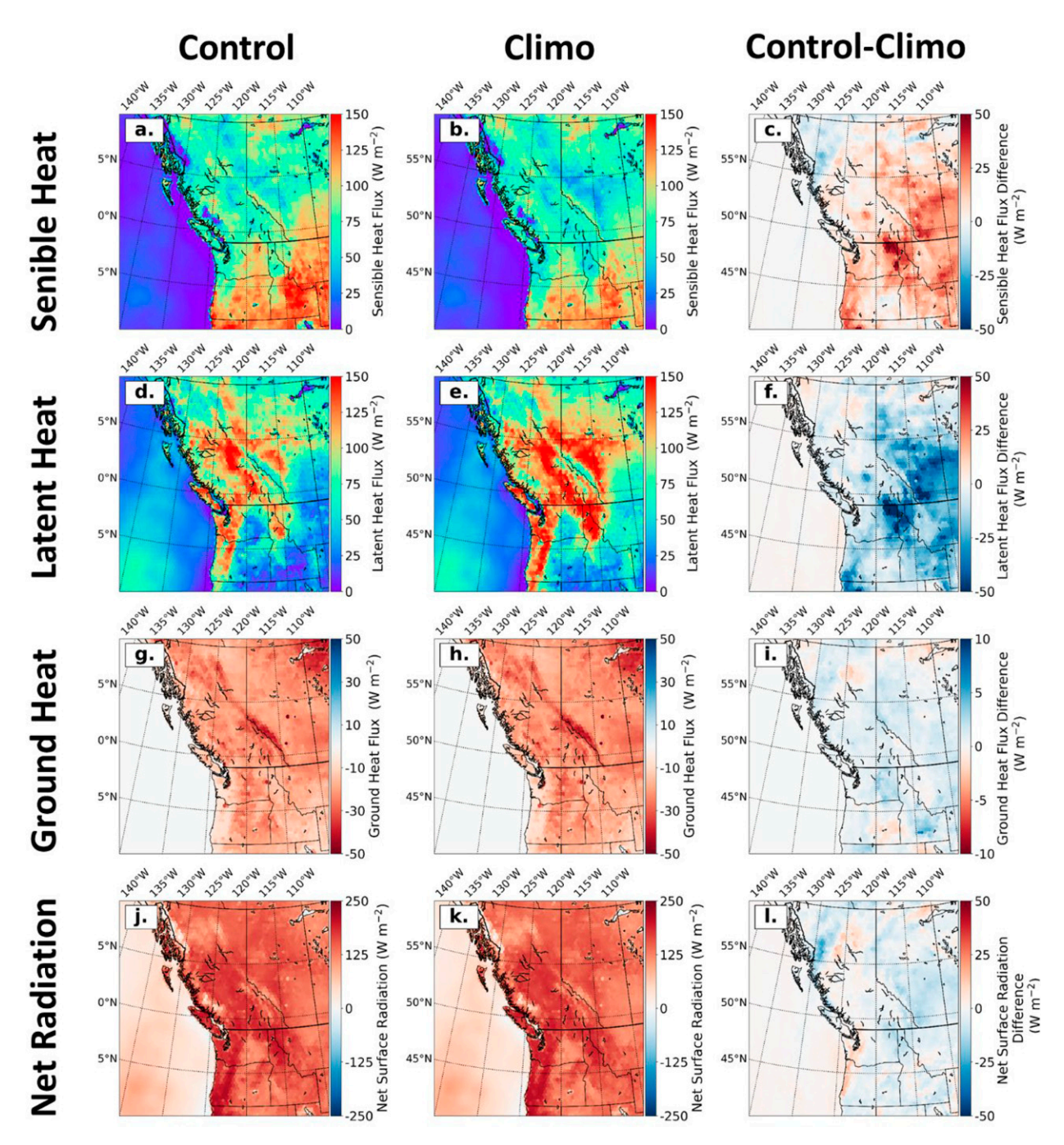


FIG. 11. Average surface heat flux and net radiation differences for 0000 UTC 27 Jun-0000 UTC 1 Jul from (left) the Control simulation, (center) the Climo simulation, and (right) their difference.

lowest \sim 150 hPa of the atmosphere. Eastern Washington, northern Oregon, and southern British Columbia experienced the largest pressure change due to soil dryness (0.5–0.8 hPa; Fig. 14). Most of the remainder of the region encompassed by the inner 4-km WRF domain experienced lower mean surface pressure in the Control simulation as well.

The lower surface air pressure in the drier Control simulation was paralleled by a decline of 5–10 m in the geopotential heights

at 925 and 850 hPa (Fig. 15). With the drier Control simulation having lower surface air pressure and lower geopotential heights centered on eastern Washington and southern British Columbia, low-level Control minus Climo wind differences resulted. For example, 925- and 850-hPa winds across the Washington Cascades were more westerly in the Control than the Climo simulation, with magnitudes generally 0.5–1.5 m s⁻¹ (Figs. 15a,b). Interestingly, this suggests that the easterly downslope winds that

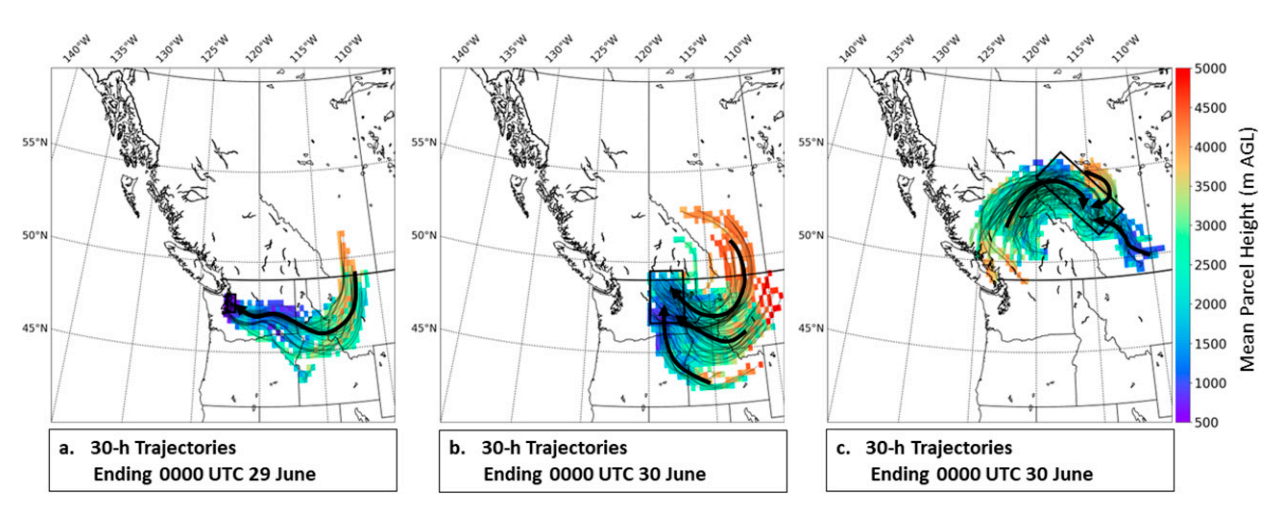


FIG. 12. The 30-h backward trajectories ending 500 m AGL over (a) Puget Sound, (b) eastern Washington and southern British Columbia, and (c) western Alberta. The color fill indicates the mean parcel height binned over 0.33° longitude and latitude. Subjectively analyzed representative airstreams are marked by bold black arrows.

impacted areas west of the Cascades (e.g., Puget Sound, WA and Portland, OR) and that contributed to downslope warming in western Washington, were slightly weaker under dry soil moisture conditions.

c. Changes along the Pacific coast of Washington and Oregon

Lower air pressure in the Control simulation affected mesoscale airflows along the Pacific coast of Washington and Oregon. Specifically, the northward progression of the alongshore surge of cool, cloudy marine air was faster in the Control than in the Climo simulation. Figure 16 shows the boundaries between clear and cloudy skies⁸ over the period when the alongshore surge moved northward along the Oregon and Washington coasts (0600 UTC 28 June–0600 UTC 29 June). The faster marine push in the Control simulation resulted from lower surface pressure over eastern Washington (Fig. 14), which strengthened onshore pressure gradients and accelerated the marine air northward along the coast. Because of the faster influx of marine air, air temperatures along the coast were briefly cooler (1–3 h; 2°–10°C) in the Control than in the Climo simulation.

5. Conclusions

The goal of this study was to examine the role of soil moisture during the record-breaking North American heatwave in late June 2021. This heatwave produced all-time record high temperatures across large swaths of northwestern North America, including along the Pacific coastal zone where air temperatures are usually moderated by nearby cool ocean water. The event was forced by anomalous 500-hPa ridging, which exceeded $+3\sigma$ above climatology, leading to intense

lower-tropospheric subsidence warming and downslope winds on the lee slopes of regional mountain ranges. Temperature anomalies during the event were amplified by synoptic- and mesoscale subsidence over large portions of Washington, Oregon, British Columbia, and Alberta.

At the start of the heatwave on 26 June 2021, soil moisture levels were significantly below normal across most of Washington, Oregon, British Columbia, and Alberta. Four to six months before the heatwave, there was near- or above-normal precipitation across most of this region, followed by a precipitation deficit during the spring that contributed to a steady drying until mid-June. A brief period of rainfall in mid-June temporarily boosted soil moisture to above-normal levels over portions of Washington and British Columbia before rapidly drying between the middle and end of June.

Soil moisture can significantly modulate heatwaves by altering the energy balance at the surface of Earth, leading to warmer near-surface air temperatures when soil is drier (less evaporative cooling and greater sensible heat flux). To examine the impacts of soil moisture on this heatwave event, two simulations were compared. The first experiment, called the Control,

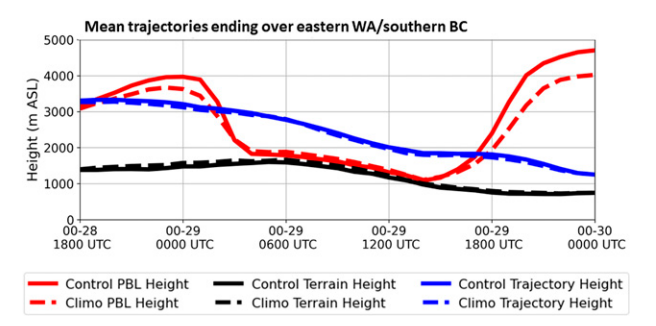


FIG. 13. Time series of 30-h backward mean trajectories ending 500 m AGL over eastern Washington and southern British Columbia. Colored lines indicate the boundary layer height (red), terrain height (black), and trajectory height (blue). Dashed (solid) lines are from the Climo (Control) simulation.

⁸ Cloudy skies are defined as areas where the simulated cloud fraction exceeds 10%.

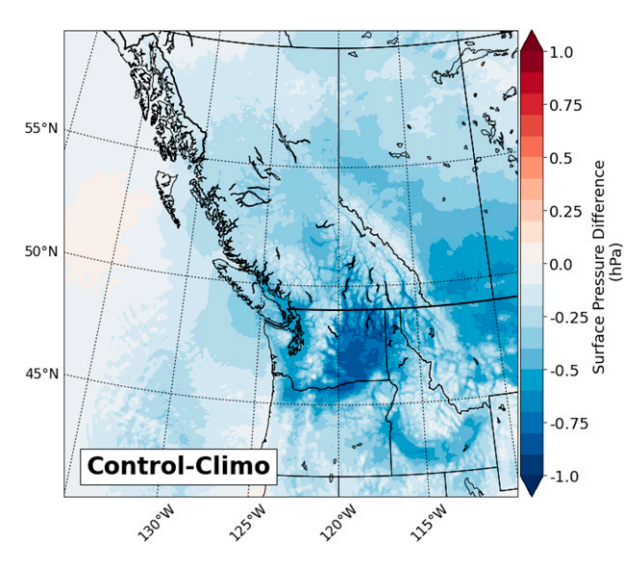


FIG. 14. Surface pressure difference (Control minus Climo) averaged over the 0000 UTC 27 Jun–0000 UTC 1 Jul period.

used observed soil moisture conditions from the Global Land Data Assimilation System (GLDAS) to replicate the actual soil conditions at model initialization. The second experiment, called the Climo simulation, initialized the model using the 1980–2020 climatological GLDAS soil moisture, which was moister than the Control. Both experiments simulated the period from 1200 UTC 26 June to 1200 UTC 2 July 2021.

Low-level (2-m) air temperatures over Washington, Oregon, British Columbia, and Alberta averaged 0.48°C warmer in the drier Control compared to the Climo simulation. The greatest magnitude of temperature increase was over eastern Washington and southern British Columbia, coinciding with the region of largest soil moisture differences, with 0000 UTC temperatures averaging 1.84°C warmer in the Control than the Climo simulation. The warming of 0.5°–2.5°C (1%–6%) was relatively small, consistent with previous studies that suggest that northwestern North America is not region where significant land–atmosphere feedbacks are expected (Koster et al. 2004; Dirmeyer et al. 2016, 2022).

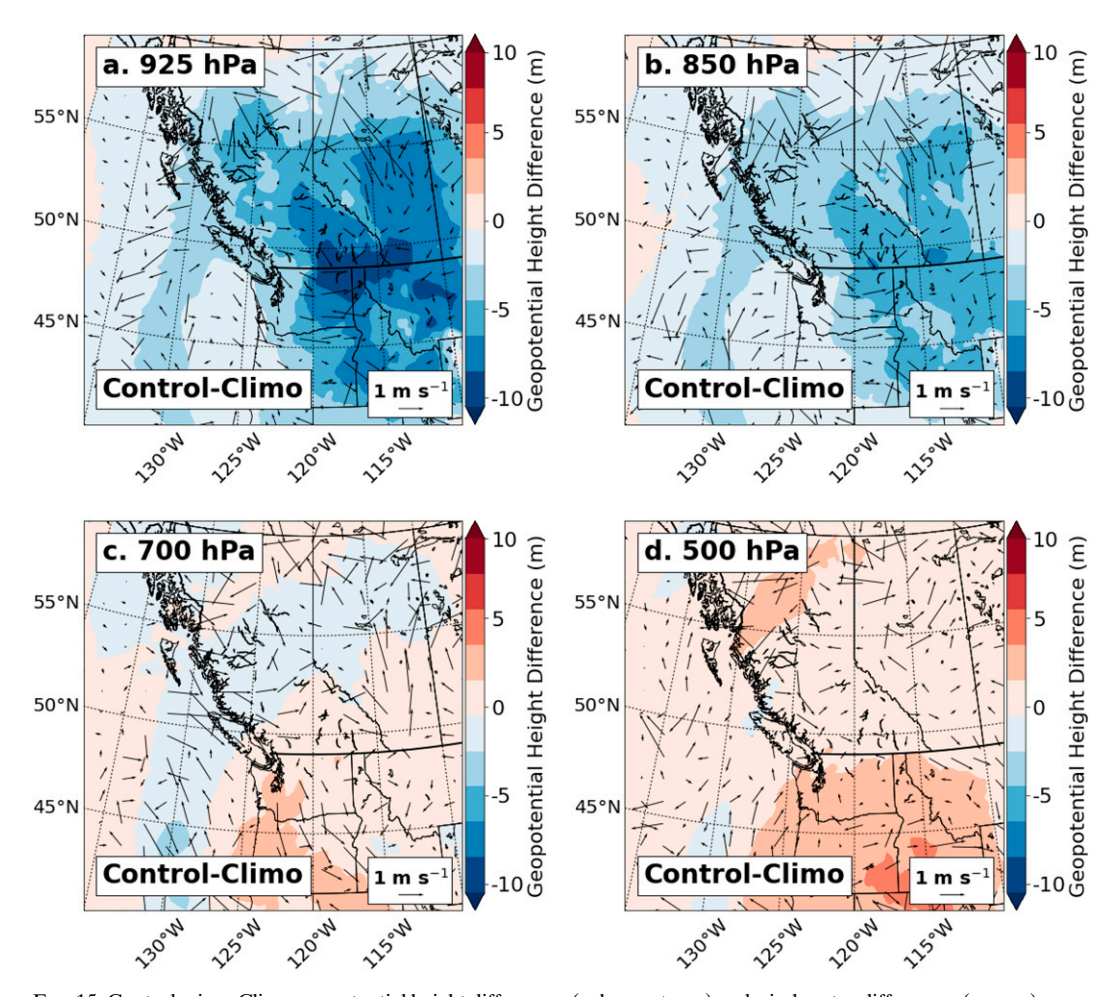


FIG. 15. Control minus Climo geopotential height differences (color contours) and wind vector differences (arrows) averaged over the 0000 UTC 27 Jun–0000 UTC 1 Jul period at standard levels.

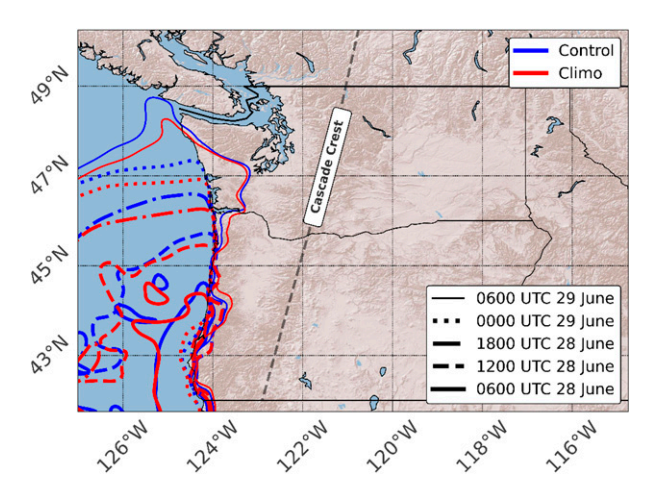


FIG. 16. Alongshore surge progression during the 24-h period from 0600 UTC 28 Jun to 0600 UTC 29 Jun 2021 from the Control (blue) and Climo (red) simulations. Line styles indicate times at 6-h intervals.

Analysis of air parcel trajectories and consideration of latent and sensible heat flux differences demonstrated that air parcels ending at the surface on the hottest days of the heatwave began at high altitudes (often above 3 km MSL) and remained well above the influence of boundary layer processes until the last \sim 6 h of the trajectories when strong subsidence brought the parcels to the surface. Thus, the impact of altered boundary layer processes on surface temperatures was relatively small.

In the Control simulation, regions of anomalously dry soils corresponded not only to anomalous low-level warmth, but also to lower surface air pressure. Furthermore, the lower surface air pressure coincided with lower geopotential heights below 700 hPa across the same regions. Finally, comparisons of pressure, temperature, and cloud cover between the simulations showed that the northward progression of the heatwave-ending alongshore marine surge was faster in the Control than the Climo simulation.

To summarize, this study suggests that the June 2021 heatwave over northwestern North America was 0.5° – 2.5° C warmer as a result of abnormally dry soil moisture conditions before and during the event. Evaluation of surface heat fluxes and air parcel trajectories suggest that the effects of soil moisture were lessened due to air parcels' short time in the boundary layer, which limited the effects of surface fluxes. As a result, dry antecedent soil moisture conditions only made a small contribution to the high-amplitude June 2021 heatwave. It is important to note that model configuration choices may affect the sensitivity of air temperature to soil moisture. As part of our experiments, we did find modest differences air

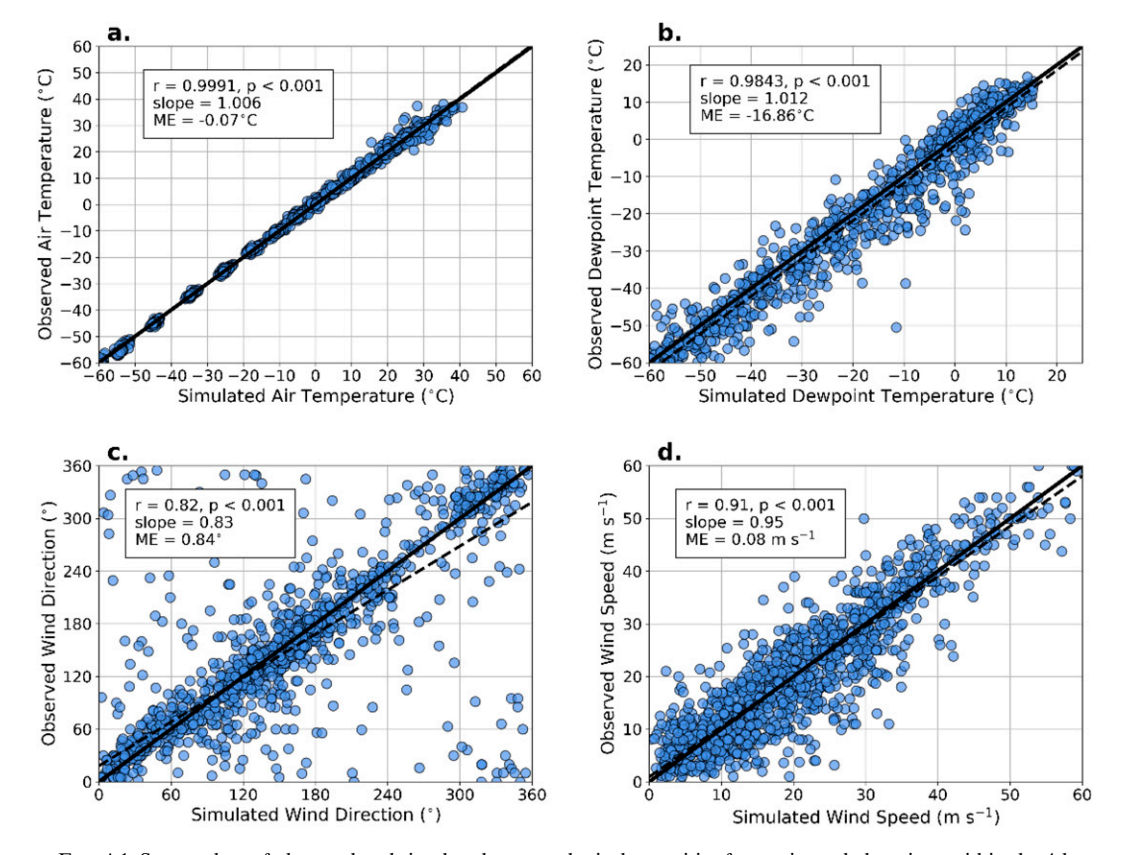


FIG. A1. Scatterplots of observed and simulated meteorological quantities for rawinsonde locations within the 4-km WRF domain (a) air temperature, (b) dewpoint temperature, (c) wind direction, and (d) wind speed. Each panel also provides linear correlation (r) and mean error (ME) statistics.

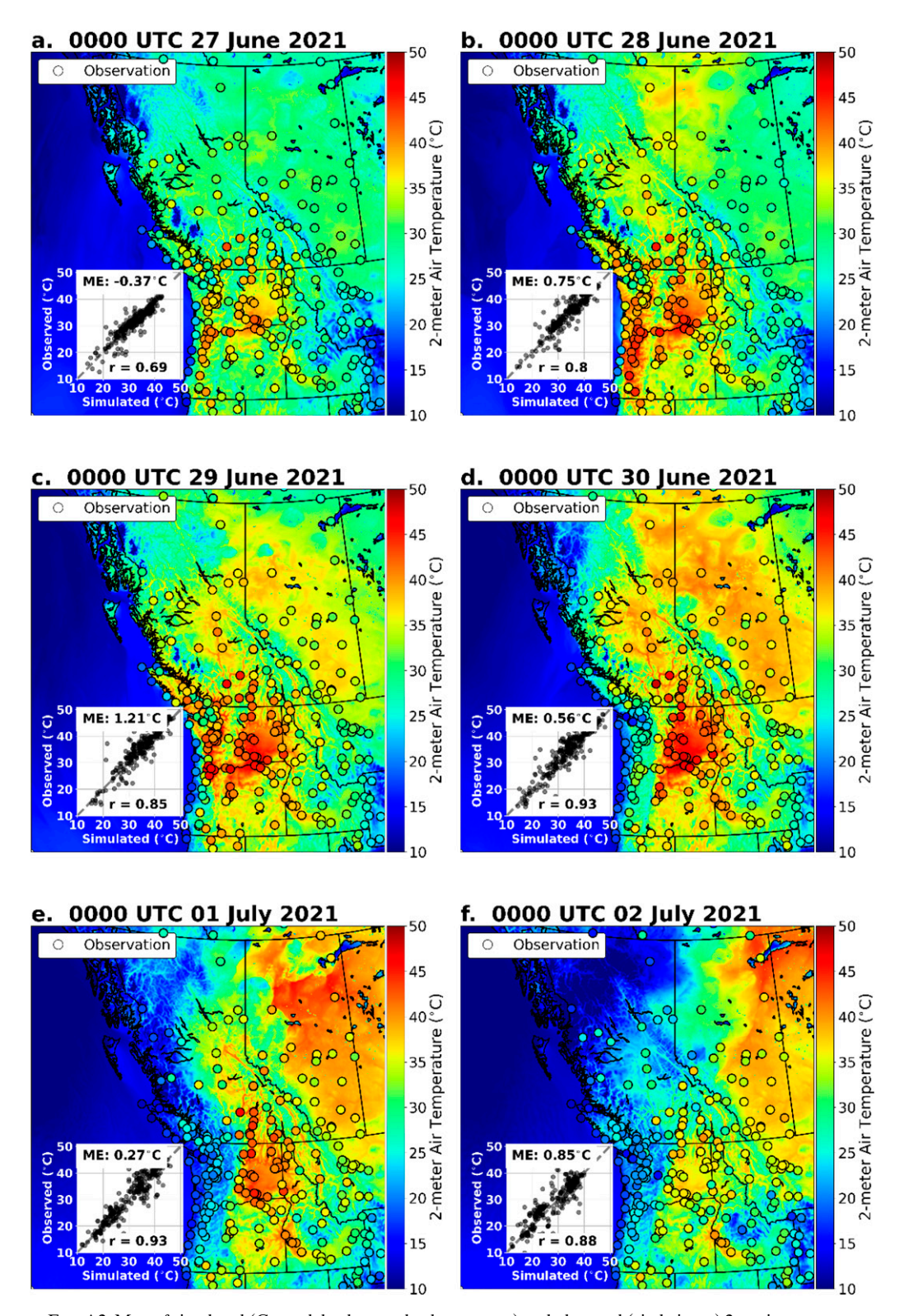


FIG. A2. Map of simulated (Control; background color contour) and observed (circle icons) 2-m air temperature at 0000 UTC each day of the simulation. The lower-left inset in each panel shows a scatterplot of the data, with the correlation coefficient (*r*) and mean error (ME) shown.

temperature sensitivity that resulted from different model configurations. As with any modeling study, sensitivity of results can be affected by a number of factors, including the choices of initial conditions (e.g., soil moisture), model domain configuration, model physical parameterizations (e.g., the land surface model), or a combination thereof. Finally, the authors suggest that future work investigate the generality of these results by assessing the impact of soil moisture on other events in the region.

Acknowledgments. The authors acknowledge partial support from NSF Grant AGS-2042105 and thank Dr. Joseph Boomgard-Zagrodnik for early project consultation. The authors also thank the anonymous reviewers whose comments helped to greatly improve the manuscript.

Data availability statement. All data used in this manuscript are freely available at the following sources or by request from the corresponding author, including the following: WRF Model data, including namelists, are available upon request. GFS grids for model initialization are available from the National Centers for Environmental Information (NCEI): https://www.ncei.noaa.gov/products/weather-climate-models/global-forecast. NARR grids can be obtained through the NCEI: https://www.ncei.noaa.gov/products/weather-climate-models/north-american-regional. ERA5

grids can be obtained through the Copernicus Climate Data Store: https://cds.climate.copernicus.eu/. Rawinsonde vertical profiles can be obtained through the University of Wyoming website: http://weather.uwyo.edu/upperair/sounding.html. GLDAS soil moisture data: https://ldas.gsfc.nasa.gov/.

APPENDIX A

Control Simulation Fidelity

Observed and simulated air temperature, dewpoint temperature, wind speed, and wind direction from rawinsonde sites located within the 4-km WRF domain (locations in Fig. 7) are evaluated using scatterplots in Figure A1. Simulated and observed 0000 and 1200 UTC conditions are assessed from 1200 UTC 26 June to 1200 UTC 1 July 2021. Profiles are linearly interpolated every 50 hPa from 1000 to 50 hPa.

All four fields show strong correlations between observed and simulated quantities, with temperature, dewpoint temperature, and wind speed correlation coefficients exceeding 0.9. Wind direction was similarly well-simulated, though timing differences associated with the marine push along the coast reduced the correlation coefficient between simulated and observed wind direction to r=0.82. However, if the outliers are removed, the correlation exceeds 0.9. Next,

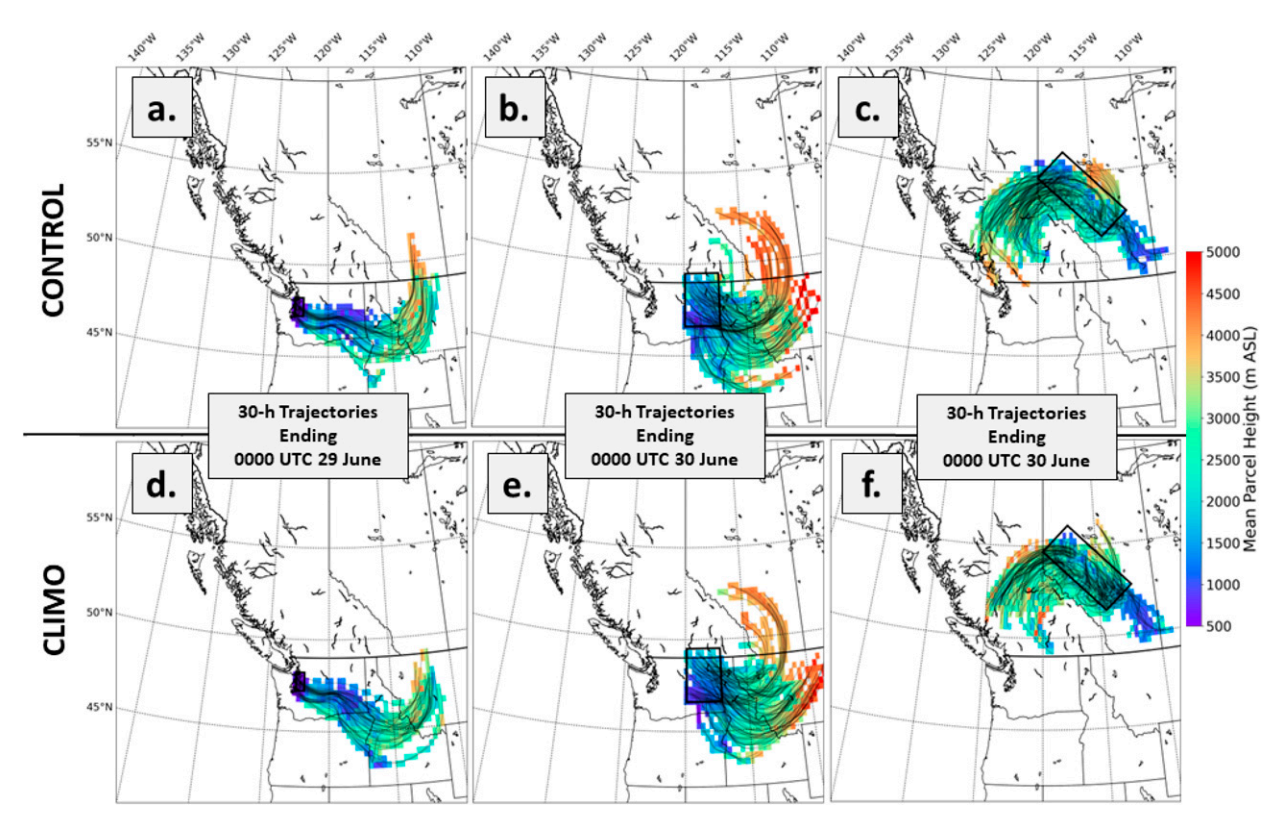


FIG. B1. The 30-h backward trajectories ending 500 m AGL over (a),(d) Puget Sound; (b),(e) eastern Washington and southern British Columbia; and (c),(f) western Alberta. Rows show trajectories from the (top) Control and (bottom) Climo simulations. The color fill indicates the mean parcel height binned over 0.33° longitude and latitude.

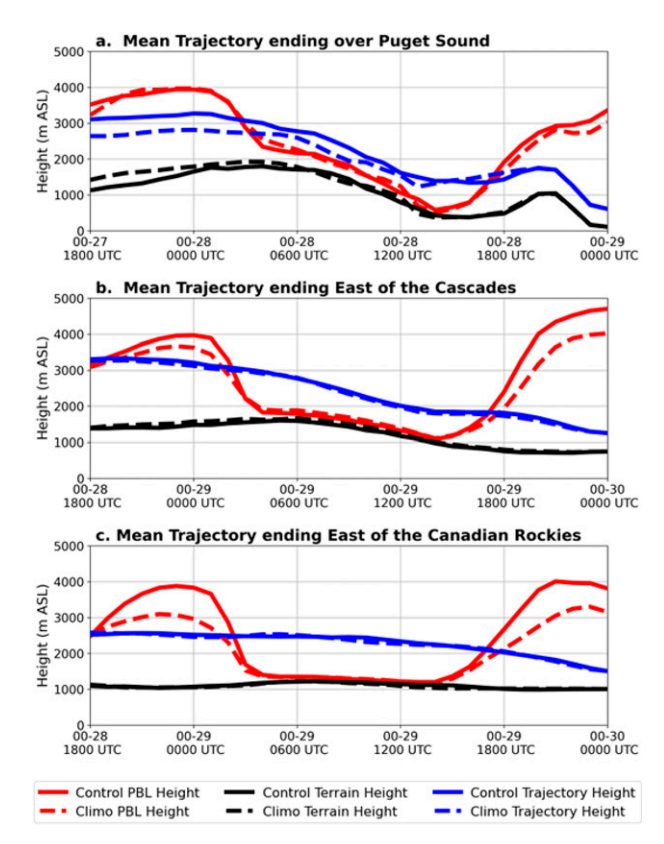


FIG. B2. Time series of 30-h backward mean trajectories ending 500 m AGL over (a) Puget Sound, (b) eastern Washington and southern British Columbia, and (c) western Alberta. Ending locations are shown in Fig. 7. Colored lines indicate the boundary layer height (red), terrain height (black), and trajectory height (blue). Dashed (solid) lines are from the Climo (Control) simulation.

2-m air temperatures at stations across the 4-km domain are evaluated. Considering the 0000 UTC air temperatures, which corresponds approximately with the warmest time of the day (1600–1700 LST), mean errors ranged between -0.37° and 1.21°C, with realistic simulated temperature distributions across the domain (Fig. A2). Scatterplots of simulated versus observed temperatures show high correlations (0.69–0.93), with simulation-observation pairs clustered around the one-to-one line. Correlations between simulated and observed 2-m air temperatures are highest during the peak of the heatwave (28 June–1 July). Combining the above evaluations, we can conclude that low-level air temperatures and synoptic conditions were skillfully and realistically simulated by the Control simulation.

APPENDIX B

Simulated Trajectory Analysis

This appendix provides additional information regarding the simulated trajectories presented in section 4. Figure B1 trajectories from the Control and Climo simulations ending over Puget Sound, eastern WA/southern BC, and western AB. Trajectories from both simulations were similar in their starting locations, paths taken, and parcel heights MSL along the trajectory paths. There were, however, some minor differences. First, air parcels in the warmer and drier Control simulation followed a more northerly trajectory than those in the cooler and wetter Climo simulation. Second, air parcels in the Control simulation tended to start at a higher altitude than those in the Climo simulation. Both of these differences can likely be attributed to the geopotential height changes outlined in section 4 and Fig. 15, though the differences in trajectories are generally considered minor.

The mean behavior of the three sets of 30-h backward trajectories is shown in Figure B2 from the Control and Climo simulations, with all trajectories ending around the time of the heatwave's peak. As was the case with the trajectories ending over eastern Washington and southern British Columbia, which was shown in Fig. 13 and discussed in section 4, trajectories from both simulations followed similar paths with respect to height above terrain and height relative to the boundary layer. For all three sets of trajectories, air parcels began near or above the top of the boundary layer, then experienced a prolonged period above the boundary layer during the overnight hours, followed by a ~6-h period within the boundary layer before ending at 500 m AGL. In all three cases, air parcels were at least 500-1000 m above the surface until the last 6 h of each mean trajectory, indicating that surface fluxes were minimally affecting air parcels during their descent toward the surface.

REFERENCES

Alfaro, E. J., A. Gershunov, and D. Cayan, 2006: Prediction of summer maximum and minimum temperature over the central and western United States: The roles of soil moisture and sea surface temperature. J. Climate, 19, 1407–1421, https://doi.org/10.1175/JCLI3665.1.

Bartusek, S., K. Kornhuber, and M. Ting, 2022: 2021 North American heatwave amplified by climate change-driven nonlinear interactions. *Nat. Climate Change*, 12, 1143–1150, https://doi.org/10.1038/ s41558-022-01520-4.

Benson, D. O., and P. A. Dirmeyer, 2021: Characterizing the relationship between temperature and soil moisture extremes and their role in the exacerbation of heatwaves over the contiguous United States. *J. Climate*, 34, 2175–2187, https://doi.org/10.1175/JCLI-D-20-0440.1.

Brabson, B. B., D. H. Lister, P. D. Jones, and J. P. Palutikof, 2005: Soil moisture and predicted spells of extreme temperatures in Britain. *J. Geophys. Res.*, **110**, D05104, https://doi.org/10.1029/2004JD005156.

Cai, W., T. Cowan, P. Briggs, and M. Raupach, 2009: Rising temperature depletes soil moisture and exacerbates severe drought conditions across southeast Australia. *Geophys. Res. Lett.*, 36, L21709, https://doi.org/10.1029/2009GL040334.

Dirmeyer, P. A., and Coauthors, 2016: Confronting weather and climate models with observational data from soil moisture networks over the United States. *J. Hydrometeor.*, 17, 1049– 1067, https://doi.org/10.1175/JHM-D-15-0196.1.

—, G. Balsamo, E. M. Blyth, R. Morrison, and H. M. Cooper, 2021: Land-atmosphere interactions exacerbated the drought and

- heatwave over northern Europe during summer 2018. *AGU Adv.*, **2**, e2020AV000283, https://doi.org/10.1029/2020AV000283.
- —, R. Mantripragada, B. Gay, and D. Klein, 2022: Evolution of land surface feedbacks on extreme heat: Adapting existing coupling metrics to a changing climate. *Front. Envion. Sci.*, 10, 949250, https://doi.org/10.3389/fenvs.2022.949250.
- Durre, I., J. M. Wallace, and D. P. Lettenmaier, 2000: Dependence of extreme daily maximum temperatures on antecedent soil moisture in the contiguous United States during summer. *J. Climate*, 13, 2641–2651, https://doi.org/10.1175/1520-0442(2000)013<2641: DOEDMT>2.0.CO;2.
- Ek, M., K. E. Mitchell, Y. Lin, E. Rogers, P. Grunmann, V. Koren, G. Gayno, and J. D. Tarpley, 2003: Implementation of the Noah land surface model advances in the National Centers for Environmental Prediction operational mesoscale Eta Model. J. Geophys. Res., 108, 8851, https://doi.org/10.1029/2002JD003296.
- Fischer, E. M., S. I. Seneviratne, P. L. Vidale, D. Lüthi, and C. Schär, 2007: Soil moisture–atmosphere interactions during the 2003 European summer heatwave. *J. Climate*, 20, 5081–5099, https://doi.org/10.1175/JCLI4288.1.
- Ford, T. W., and S. M. Quiring, 2014: In situ soil moisture coupled with extreme temperatures: A study based on the Oklahoma Mesonet. *Geophys. Res. Lett.*, 41, 4727–4734, https://doi.org/ 10.1002/2014GL060949.
- Grell, G. A., and S. R. Freitas, 2014: A scale and aerosol aware stochastic convective parameterization for weather and air quality modeling. *Atmos. Chem. Phys.*, 14, 5233–5250, https:// doi.org/10.5194/acp-14-5233-2014.
- Hersbach, H., and Coauthors, 2020: The ERA5 global reanalysis. *Quart. J. Roy. Meteor. Soc.*, **146**, 1999–2049, https://doi.org/10.1002/qj.3803.
- Hirsch, A. L., A. J. Pitman, S. I. Seneviratne, J. P. Evans, and V. Haverd, 2014: Summertime maximum and minimum temperature coupling asymmetry over Australia determined using WRF. *Geophys. Res. Lett.*, 41, 1546–1552, https://doi.org/10.1002/2013GL059055.
- Hirschi, M., and Coauthors, 2011: Observational evidence for soil-moisture impact on hot extremes in southeastern Europe. *Nat. Geosci.*, **4**, 17–21, https://doi.org/10.1038/ngeo1032.
- Hong, S. Y., Y. Noh, and J. Dudhia, 2006: A new vertical diffusion package with an explicit treatment of entrainment processes. *Mon. Wea. Rev.*, 134, 2318–2341, https://doi.org/10.1175/MWR3199.1.
- Huang, J., and H. M. van den Dool, 1993: Monthly precipitation-temperature relations and temperature prediction over the United States. *J. Climate*, 6, 1111–1132, https://doi.org/10.1175/1520-0442(1993)006<1111:MPTRAT>2.0.CO;2.
- Iacono, M. J., J. S. Delamere, E. J. Mlawer, M. W. Shephard, S. A. Clough, and W. D. Collins, 2008: Radiative forcing by long-lived greenhouse gases: Calculations with the AER radiative transfer models. J. Geophys. Res., 113, D13103, https:// doi.org/10.1029/2008JD009944.
- Jaeger, E., and S. Seneviratne, 2011: Impact of soil moisture– atmosphere coupling on European climate extremes and trends in a regional climate model. *Climate Dyn.*, 36, 1919– 1939, https://doi.org/10.1007/s00382-010-0780-8.
- Jannuzzi, J. A., 1993: The onshore push of marine air into the Pacific Northwest. Wea. Forecasting, 8, 194–202, https://doi. org/10.1175/1520-0434(1993)008<0194:TOPOMA>2.0.CO;2.
- Jia, G., and Coauthors, 2019: Land-climate interactions. Climate Change and Land, P. R. Shukla et al., Eds., Cambridge University Press, 131–247.

- Klemp, J. B., 2011: A terrain-following coordinate with smoothed coordinate surfaces. *Mon. Wea. Rev.*, **139**, 2163–2169, https:// doi.org/10.1175/MWR-D-10-05046.1.
- Koster, R. D., and Coauthors, 2004: Regions of strong coupling between soil moisture and precipitation. *Science*, 305, 1138– 1140, https://doi.org/10.1126/science.1100217.
- —, S. Schubert, and M. Suarez, 2009: Analyzing the concurrence of meteorological droughts and warm periods, with implications for the determination of evaporative regime. *J. Climate*, 22, 3331–3341, https://doi.org/10.1175/2008JCLI2718.1.
- Lakshmi, V., T. J. Jackson, and D. Zehrfuhs, 2003: Soil moisturetemperature relationships: Results from two field experiments. *Hydrol. Processes*, 17, 3041–3057, https://doi.org/10.1002/hyp.1275.
- Liu, J., and Z. Pu, 2019: Does soil moisture have an influence on near-surface temperature? J. Geophys. Res. Atmos., 124, 6444– 6466, https://doi.org/10.1029/2018JD029750.
- Mass, C. F., M. D. Albright, and D. J. Brees, 1986: The onshore surge of marine air into the Pacific Northwest: A coastal region of complex terrain. *Mon. Wea. Rev.*, 114, 2602–2627, https://doi. org/10.1175/1520-0493(1986)114<2602:TOSOMA>2.0.CO;2.
- Mazdiyasni, O., and A. AghaKouchak, 2015: Substantial increase in concurrent droughts and heatwaves in the United States. *Proc. Natl. Acad. Sci. USA*, 112, 11 484–11 489, https://doi.org/ 10.1073/pnas.1422945112.
- Meng, L., and Y. Shen, 2014: On the relationship of soil moisture and extreme temperatures in East China. *Earth Interact.*, 18, https://doi.org/10.1175/2013E1000551.1.
- Miralles, D. G., M. J. van den Berg, A. J. Teuling, and R. M. de Jeu, 2012: Soil moisture-temperature coupling: A multiscale observational analysis. *Geophys. Res. Lett.*, 39, L21707, https://doi. org/10.1029/2012GL053703.
- —, A. J. Teuling, C. C. van Heerwaarden, and J. Vilà-Guerau de Arellano, 2014: Mega-heatwave temperatures due to combined soil desiccation and atmospheric heat accumulation. *Nat. Geosci.*, 7, 345–349, https://doi.org/10.1038/ngeo2141.
- —, P. Gentine, S. I. Seneviratne, and A. J. Teuling, 2019: Land–atmospheric feedbacks during droughts and heatwaves: State of the science and current challenges. *Ann. N. Y. Acad. Sci.*, **1436**, 19–35, https://doi.org/10.1111/nyas.13912.
- Neal, E., C. S. Y. Huang, and N. Nakamura, 2022: The 2021 Pacific Northwest heat wave and associated blocking: Meteorology and the role of an upstream cyclone as a diabatic source of wave activity. *Geophys. Res. Lett.*, 49, e2021GL097699, https://doi.org/10.1029/2021GL097699.
- Overland, J. E., 2021: Causes of the record-breaking Pacific Northwest heatwave, late June 2021. *Atmosphere*, **12**, 1434, https://doi.org/10.3390/atmos12111434.
- Perkins, S., L. Alexander, and J. Nairn, 2012: Increasing frequency, intensity and duration of observed global heatwaves and warm spells. *Geophys. Res. Lett.*, 39, L20714, https://doi.org/10.1029/2012GL053361.
- Petch, J. C., C. J. Short, M. J. Best, M. McCarthy, H. W. Lewis, S. B. Vosper, and M. Weeks, 2020: Sensitivity of the 2018 UK summer heatwave to local sea temperatures and soil moisture. Atmos. Sci. Lett., 21, e948, https://doi.org/10.1002/asl.948.
- Putnam, A. E., and W. S. Broecker, 2017: Human-induced changes in the distribution of rainfall. *Sci. Adv.*, 3, e1600871, https://doi.org/10.1126/sciadv.1600871.
- Rodell, M., and Coauthors, 2004: The Global Land Data Assimilation System. *Bull. Amer. Meteor. Soc.*, **85**, 381–394, https://doi.org/10.1175/BAMS-85-3-381.

- Schwingshackl, C., M. Hirschi, and S. I. Seneviratne, 2017: Quantifying spatiotemporal variations of soil moisture control on surface energy balance and near-surface air temperature. *J. Climate*, 30, 7105–7124, https://doi.org/10.1175/JCLI-D-16-0727.1.
- Seneviratne, S. I., D. Lüthi, M. Litschi, and C. Schär, 2006: Land-atmosphere coupling and climate change in Europe. *Nature*, 443, 205–209, https://doi.org/10.1038/nature05095.
- —, T. Corti, E. L. Davin, M. Hirschi, E. B. Jaeger, I. Lehner, B. Orlowsky, and A. J. Teuling, 2010: Investigating soil moisture-climate interactions in a changing climate: A review. *Earth-Sci. Rev.*, 99, 125–161, https://doi.org/10.1016/j.earscirev.2010.02.004.
- —, and Coauthors, 2013: Impact of soil moisture–climate feed-backs on CMIP5 projections: First results from the GLACE-CMIP5 experiment. *Geophys. Res. Lett.*, 40, 5212–5217, https://doi.org/10.1002/grl.50956.
- Sheridan, S., and C. Lee, 2018: Temporal trends in absolute and relative extreme temperature events across North America. *J. Geophys. Res. Atmos.*, 123, 11889–11898, https://doi.org/ 10.1029/2018JD029150.
- Skamarock, W. C., and Coauthors, 2008: A description of the Advanced Research WRF version 3. NCAR Tech. Note NCAR/TN-475+STR, 113 pp., https://doi.org/10.5065/D68S4MVH.
- Stéfanon, M., P. Drobinski, F. D'Andrea, C. Lebeaupin-Brossier, and S. Bastin, 2014: Soil moisture-temperature feedbacks at meso-scale during summer heat waves over western Europe. *Climate Dyn.*, 42, 1309–1324, https://doi.org/10.1007/s00382-013-1794-9.
- Stein, A. F., R. R. Draxler, G. D. Rolph, B. J. B. Stunder, M. D. Cohen, and F. Ngan, 2015: NOAA's HYSPLIT atmospheric transport and dispersion modeling system. *Bull. Amer. Meteor. Soc.*, 96, 2059–2077, https://doi.org/10.1175/BAMS-D-14-00110.1.

- Taylor, C. M., R. A. de Jeu, F. Guichard, P. P. Harris, and W. A. Dorigo, 2012: Afternoon rain more likely over drier soils. *Nature*, 489, 423–426, https://doi.org/10.1038/nature11377.
- Thompson, G., P. R. Field, R. M. Rasmussen, and W. D. Hall, 2008: Explicit forecasts of winter precipitation using an improved bulk microphysics scheme. Part II: Implementation of a new snow parameterization. *Mon. Wea. Rev.*, 136, 5095– 5115, https://doi.org/10.1175/2008MWR2387.1.
- Thompson, V., and Coauthors, 2022: The 2021 western North America heat wave among the most extreme events ever recorded globally. *Sci. Adv.*, **8**, eabm6860, https://doi.org/10.1126/sciadv.abm6860.
- Wang, C. Z., J. Y. Zheng, W. Lin, and Y. Q. Wang, 2023: Unprecedented heatwave in western North America during late June of 2021: Roles of atmospheric circulation and global warming. Adv. Atmos. Sci., 40, 14–28, https://doi.org/10.1007/ s00376-022-2078-2.
- Whan, K., J. Zscheischler, R. Orth, M. Shongwe, M. Rahimi, E. O. Asare, and S. I. Seneviratne, 2015: Impact of soil moisture on extreme maximum temperatures in Europe. Wea. Climate Extremes, 9, 57–67, https://doi.org/10.1016/j.wace.2015. 05.001.
- Xu, Z., Z. Wu, H. He, X. Guo, and Y. Zhang, 2021: Comparison of soil moisture at different depths for drought monitoring based on improved soil moisture anomaly percentage index. *Water Sci. Eng.*, 14, 171–183, https://doi.org/10.1016/j.wse. 2021.08.008.
- Yu, S., Z. Yan, N. Freychet, and Z. Li, 2020: Trends in summer heatwaves in central Asia from 1917 to 2016: Association with large-scale atmospheric circulation patterns. *Int. J. Cli*matol., 40, 115–127, https://doi.org/10.1002/joc.6197.